CHINESE OPTICS LETTERS

Vol. 23, No. 1 | January 2025

Ultrastable Nd:YAG 1064-nm lasers with 2.1×10^{-16} frequency stability based on a field-programmable gate array frequency-locked system

Zhenqian Li (李振千)[1,2], Zongyu Lu (芦宗昱)[1], Lingfeng Wan (万凌风)[1], Yuan Ru (茹 媛)[1,2], Lisheng Chen (陈李生)[1,2,3], and Liufeng Li (李刘锋)[1,3*]

[1] Innovation Academy for Precision Measurement Science and Technology, Chinese Academy of Sciences, Wuhan 430071, China

[2] University of Chinese Academy of Sciences, Beijing 100049, China

[3] State Key Laboratory of Magnetic Resonance and Atomic and Molecular Physics, Wuhan 430071, China

*Corresponding author: liufengli@apm.ac.cn

Received May 20, 2024 | Accepted July 12, 2024 | Posted Online February 4, 2025

Ultrastable continuous-wave lasers are one of the important elements for space-based gravitational wave detection. Here we present a Pound–Drever–Hall laser frequency-locked system based on a field-programmable gate array, demonstrating its potential to achieve 10^{-16} levels of frequency stability for space applications. The system is employed to lock a space-qualified 1064-nm neodymium-doped yttrium aluminum garnet laser to a laboratory-operated 20-cm ultrastable optical cavity. Major noise contributors are identified as laser intensity fluctuation and residual amplitude modulation. The heterodyne beat measurement shows that the frequency noise spectral density of a single laser is reduced to 2.5 Hz/$\sqrt{\text{Hz}}$ at a Fourier frequency of 1 mHz, and the frequency instability is 2.1×10^{-16} at 1 s and remains below 3.5×10^{-16} up to 6000 s.

Keywords: narrow-linewidth laser; automatic frequency stabilization; gravitational wave detection.
DOI: 10.3788/COL202523.011402

1. Introduction

Lasers with high-frequency stability[1] play an indispensable role in many precision measurements such as gravitational wave (GW) detection[2,3], optical frequency standards[4,5], and test of Lorentz invariance[6]. The past two decades have witnessed significant improvements in ultrastable continuous-wave (CW) lasers in terms of portability[7], footprint, and control automation[8–12]. In recent years, automatic laser frequency locking has progressively evolved from analog modules to analog–digital hybrid systems[8–10], and then to all-digital controllers[11,12] based on a field-programmable gate array (FPGA). The FPGA-based frequency-locked system has the advantages of high speed and great adaptability. Nevertheless, their noise properties at Fourier frequencies down to 1 mHz or even lower need to be quantitively examined for many applications relying on effective control of low-frequency noises. Meanwhile, replacing the free-space optical components with their optical-fiber counterparts in frequency-locked optics is another development trend to lower the weight and enhance the reliability. Being a key component in the all-fiber frequency-locked optics, a waveguide electro-optic modulator (EOM) generates unwanted amplitude modulation[13] whose impact and suppression should be further investigated.

With the technological advance of space-based gravitational wave (GW) detection, there is an increasing demand for spaceborne ultrastable lasers. Known for their exceptionally low noise, 1064 nm neodymium-doped yttrium aluminum garnet (Nd:YAG) lasers built upon nonplanar ring oscillators (NPROs) are primary laser sources in planned LISA-like GW detectors. Nevertheless, in these detectors with unmatched baselines of millions of kilometers, the frequency noise of a free-running laser, if untreated, results in a background that overwhelms the GW signal by approximately 11–12 orders of magnitude. To reach the targeted detection sensitivities, two measures are taken jointly to cope with the laser frequency noise. First, prestabilizing the laser onboard the spacecraft is done to suppress its frequency noise to 30 Hz/$\sqrt{\text{Hz}}$ (1 mHz–1 Hz)[14–17]. Subsequently, the influence of the residual frequency noise is further reduced by 7–8 orders of magnitude by adopting time-delayed interferometry (TDI)[18–22]. Effective suppression of laser frequency noise during the prestabilization phase is one of the major technological challenges for LISA-like space programs of GW detection.

In response to the demand for ultrastable lasers suitable for GW detection in space, we are developing a spaceborne 1064 nm ultrastable laser. One of the crucial steps in this task is to verify

© 2025 Chinese Optics Letters

the noise performance of the control unit adopting the FPGA architecture. We developed two independently operated laser stabilization systems, each of which consists of an FPGA-based control unit and a spaceborne 1064 nm NPRO Nd:YAG laser[23]. The Nd:YAG laser is frequency-locked to a laboratory-operated 20-cm ultrastable reference cavity[24] using the Pound–Drever–Hall (PDH) method[25]. To adapt to space applications, optical fibers and fibered components are introduced to the PDH locked optics. The current configuration allows a rigorous evaluation of the FPGA approach to a frequency-locked system with ultralow noise suitable for space GW detection. Two major noise sources, the laser intensity fluctuation and residual amplitude modulation (RAM) generated by the waveguide EOM, are suppressed by implementing additional feedback control loops, and their individual contributions to the frequency noise are measured. The laser frequency stability up to a few thousand seconds is evaluated using the optical heterodyne beat of the two locked NPRO Nd:YAG lasers.

2. Apparatus

The experimental setup for laser frequency stabilization is shown in Fig. 1. Two nearly identical systems, referred to as West and East hereinafter, are built and are independently operated, allowing performance verification via beat frequency measurement. In each system, a spaceborne Nd:YAG laser[23] is locked to an ultrastable optical reference cavity[24] with a length of 20 cm and a finesse on the order of 400,000, using the PDH frequency stabilization technique. The spacer and two mirrors of the cavity are made of Corning ultralow expansion glass (ULE) and fused silica (FS), respectively. The input mirror of the cavity

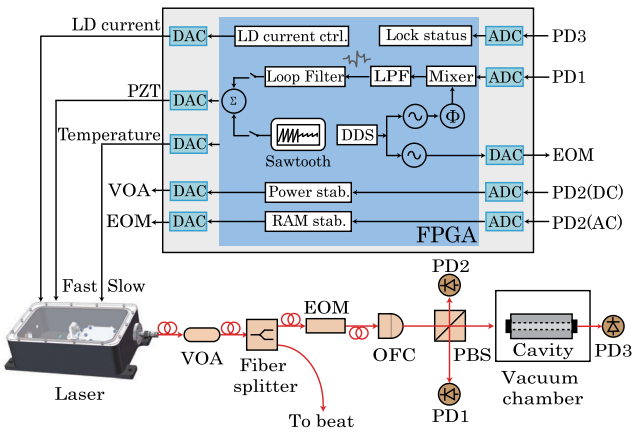

Fig. 1. Schematic diagram of the FPGA-based frequency stabilization system. Mode-matching lenses in front of the PBS and a quarter-wave plate between the PBS and cavity are not shown in the figure. VOA, variable optical attenuator; EOM, electro-optic modulator; OFC, optical fiber collimator; PD, photodetector; PBS, polarization beam splitter; FPGA, field-programmable gate array; PZT, piezo-electric transducer; DAC, digital-to-analog converter; ADC, analog-to-digital converter; DDS, direct digital synthesizer; LPF, low-pass filter; LD, laser diode.

is flat and the other one is concave [radius of curvature (ROC), 1 m]. Except for a polarization beam splitter (PBS) and a quarter-wave plate, fibered optical components are used, including an electronic variable optical attenuator (VOA), a beam splitter, and a waveguide EOM (iXblue NIR-MPX-LN-0.1), which are interconnected by polarization-maintaining (PM) single-mode fiber-optic patch cables. The laser beam first passes the VOA for optical intensity stabilization and then is divided into two beams; one beam is used to beat against the second laser, and the other is phase-modulated and subsequently coupled into the reference cavity through an optical fiber collimator (OFC). The reflected light from the cavity is guided to a photodetector (PD1) whose output is sent to the FPGA control unit for frequency demodulation.

The FPGA (Xilinx, Virtex-5) board provides a total of 5 digital-to-analog converters (DACs) and 11 analog-to-digital converters (ADCs). All DACs are 14-bit and run at a sampling rate of 100 Msps. Among the 11 ADCs, there are two high-speed ones of 16 bit, 130 Msps and 14 bit, 40 Msps that are used for sampling radio frequency (RF) signals; the rest are low-speed ones consisting of two subsets of 14 bit, 3 Msps and 12 bit, 1 Msps. Circuits realizing the functional blocks shown in Fig. 1 are laid out on the FPGA board based on a control program written in Verilog hardware description language. Emulating a payload controller, a separate board based on a microprocessor (STM32) is used to perform control and monitoring functions through serial communications with the FPGA board.

The FPGA circuit is configured to perform three major tasks, which are laser driving, frequency locking, and stabilization of laser intensity and RAM. The laser driving module stabilizes the temperature of the NPRO and controls the current of two 808-nm laser diodes pumping the NPRO. In the frequency-locked module, direct digital synthesis (DDS) is adopted to facilitate the modulation, demodulation, and frequency sweep. A sinusoidal signal (2.5 and 2.4 MHz in West and East systems, respectively) is generated by DDS and sent to EOM for phase modulation; its phase-adjustable replica serves as a local. The alternating current (AC) output of PD1 is sampled by the 16-bit ADC, which runs at a slightly reduced sampling rate of 100 Msps. The real-time data from ADC are multiplied by the digital local and then digitally filtered, resulting in frequency discrimination as the input of a digital loop filter for gain compensation. The analog actuation signal is delivered by the 14-bit DAC and applied to a piezoelectric transducer (PZT) attached to the NPRO. Parallel to the fast PZT channel, there is a slow one that works by adjusting the set point to which the temperature of NPRO is stabilized, enabling a much larger frequency tuning range. A low-frequency (2 Hz) sawtooth signal can be superimposed on the frequency actuation signal or act alone on the PZT, allowing the search of the cavity resonance or diagnosis of the PDH error signal.

Additional feedback control loops are implemented to suppress the laser intensity noise and RAM. The intensity of the laser is measured by PD2 whose direct current (DC) output is digitized by an ADC (14 bit, 3 Msps) and compared with a preset value. The resulting error signal is processed by a digital

proportional-integral-derivative (PID) controller and then converted to an analog signal that drives the VOA to actively stabilize the laser intensity. For RAM suppression, instead of using two channels that control both the bias voltage and the temperature of the EOM[13], here only the bias voltage is actively adjusted in the feedback control loop. The EOM-generated RAM is measured by PD2, whose AC output is sampled by the 14-bit, 40 Msps ADC; the downstream RAM-suppressing hardwire on the FPGA board follows the same design for the frequency locking. The feedback loop is formed by adding a DC bias voltage to the modulating signal through a bias tee, canceling the RF fundamental component emerging from the AC output of PD2. Before closing this control loop, the DC bias is set to a value at which a local maximum of the discrimination slope is reached. Meanwhile, the RAM is maximized by varying the phase of the local. This initialization process allows a long-term uninterrupted feedback control of RAM.

3. Frequency Control Algorithm

The frequency search is realized by a combination of temperature and voltage scans. First, the FPGA board initiates a bidirectional search by varying the temperature of the NPRO, which exhibits a frequency-temperature dependence of 3.1 GHz/°C and a time constant of ~1 s. The temperature scan consists of large and small steps corresponding to frequency changes of 12 and 1.5 MHz, respectively, covering a frequency range of ~6 GHz or equivalently 8 free spectral ranges (FSRs) of the 20-cm cavity. The cavity transmission, detected by PD3, is used to determine whether a resonance of TEM_{00} mode is encountered during the temperature scan. The temperature is scanned by first using the large step; if a cavity resonance occurs, the scanning step is switched to the small one. Once the resonance is within the capture range of the PZT, the temperature scan stops, and the PZT voltage scan takes over to locate the center of the resonance and prepare for a lock.

Figure 2 shows representative signals recorded during the PZT voltage scan, frequency locking, and locked state. At a rate of 2 Hz and with an actuation coefficient of 1 MHz/V, the PZT repeatedly actuates frequency sweeps of 20 MHz (peak to peak) during which the cavity transmission is continuously monitored by PD3. The resonance is confirmed when an increase in the cavity transmission occurs in four consecutive sweeps, and the frequency sweep is reduced to 2.5 MHz. Otherwise, the NPRO temperature is fine-tuned with a step size corresponding to a frequency change of 300 kHz, relocating the transmission peak to the middle of the PZT voltage scan. The voltage scan continues until the transmission signal reaches a preset value (here, 100 mV), and the PZT feedback control loop is closed. The gain of the control loop is compensated by the digital loop filter adopting an incremental PID algorithm; the bandwidth of the control loop is ~10 kHz.

In the locked state, the voltage applied to PZT will eventually saturate due to the long-term drifts of NPRO and cavity. Every 3 s, this voltage is queried, and if the voltage exceeds ±5 V, then

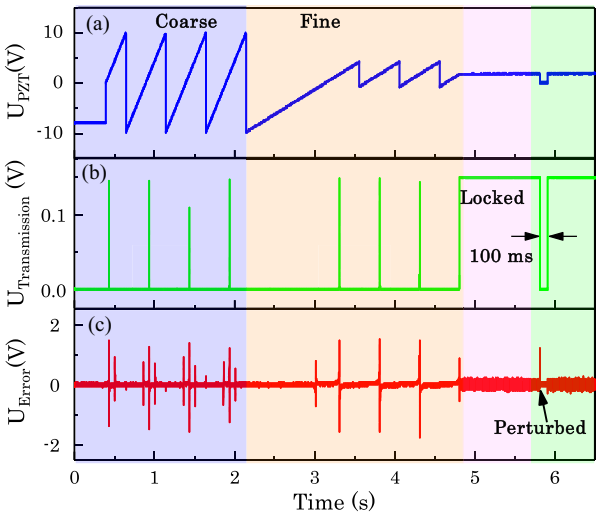

Fig. 2. (a) PZT actuation, (b) cavity transmission, and (c) error signal during the establishment of laser frequency locking. The coarse and fine PZT voltage scans cover frequency ranges of 20 and 2.5 MHz, respectively. Around 5.8 s, a perturbation is introduced and the locking is recovered after 100 ms.

it is pulled back by fine-tuning the NPRO temperature, thus preventing the PZT from being overburdened. The NPRO has a mode-hop-free temperature tuning range of about 15 GHz, which is large enough for uninterrupted long-term locking. An anti-jamming mechanism[26] is added to the locked state in which if a glitch appears in the error signal, the loop filter enters a 100-ms holding mode in which the input is disconnected and the output is latched on to the value at the sight of the interference. This approach allows a fast recovery from strong perturbations, and in Fig. 2 its effectiveness is demonstrated by the signals around 5.8 s.

4. Noise Analysis

Figure 3(a) shows the in-loop noises of the PDH frequency locking in West and East systems, together with the electronic noise and shot noise. The noises are measured at the demodulation output and then converted to frequency noises using the discrimination coefficients, which are 4.7×10^{-5} V/Hz and 6.9×10^{-5} V/Hz in West and East systems, respectively. At ~100 Hz and towards higher Fourier frequencies, the in-loop noise bumps up (servo bump), resulting in an elevated noise in the error signal when the frequency control loop is closed [Fig. 2(c)].

Due to the photothermal effect, the fluctuation of the intracavity optical power induces changes in the cavity length, thereby influencing the frequency stability of the locked laser. The optical power entering the cavity is 150 μW, and the frequency-power dependences of the West and East cavities are measured to be 2.2 and 3.8 Hz/μW, respectively. While PD2 is used for intensity stabilization, the DC output of PD1 is recorded for out-of-loop evaluation of the relative intensity noise (RIN). With intensity stabilization, the RIN measured by PD1 is reduced to $8 \times 10^{-3}/\sqrt{\text{Hz}}$ (100 μHz) − $4.0 \times 10^{-4}/\sqrt{\text{Hz}}$ (0.5 Hz) in the

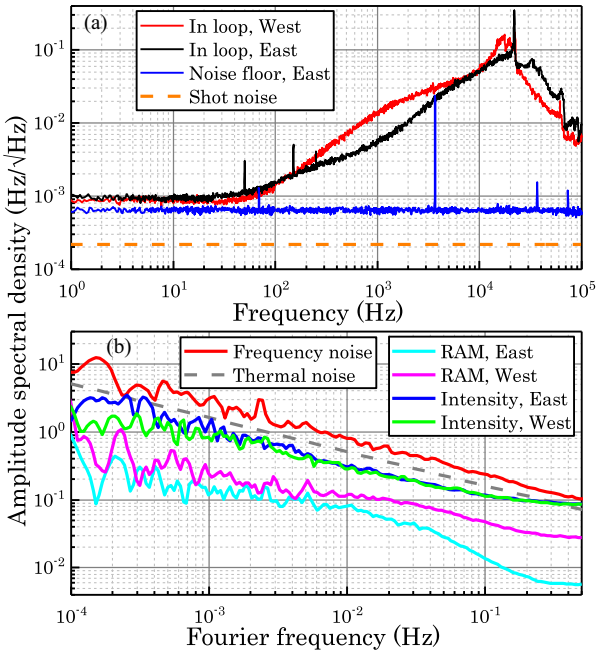

Fig. 3. Laser frequency noise and individual noise contributions. (a) In-loop noise of PDH frequency locking and the noise floor of electronic origin. (b) Laser frequency noise and contributions from RIN and RAM. The noise floor is measured by blocking the beam impinging on PD1 and then measuring the demodulated signal. The frequency noise spectrum is obtained from 12-h data of heterodyne beat between two locked Nd:YAG lasers, and individual noise contributions from laser intensity fluctuation and RAM are from separate out-of-loop measurements. Digital low-pass filters with a corner frequency of 1 kHz are used for the RAM measurements.

West system, and a similar result is obtained in the other system. Figure 3(b) shows the resulting frequency noises in the two systems, estimated by the power sensitivities mentioned above. At 1 mHz, RIN contributes a frequency noise of 1 $\mathrm{Hz}/\sqrt{\mathrm{Hz}}$, which is below the thermal noise originating from the optical cavity.

The RAM generated by the EOM is also one of the main sources of frequency noise in the PDH frequency locking. Although the waveguide of EOM is prepared with a proton exchange process to only allow extraordinary light to propagate[27], we observe a nonzero amplitude modulation on the level of 50 ppm. This RAM is found to vary with the temperature and the DC bias voltage applied to the electrodes of EOM, a phenomenon that matches the signature of birefringence interference that has been thoroughly investigated[28]. Figure 3(b) shows the RAM-induced frequency noises measured in the two systems when the feedback control of RAM is implemented. PD1 is used for RAM detection when the cavity is off-resonant, and the demodulated signals are converted to frequency noises using the corresponding PDH discrimination coefficients. Thanks to the flexibility of adding extra digital feedback control loops realized by the FPGA approach, the RAM-induced frequency noise has been reduced to be well below the cavity thermal noise in a wide spectral range from 100 μHz to 0.5 Hz.

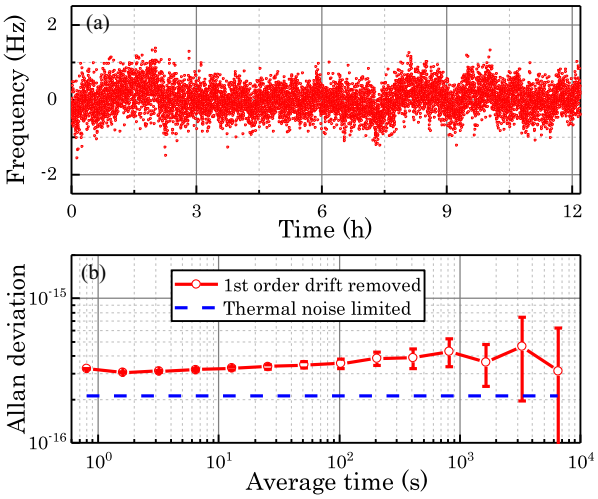

Fig. 4. Optical heterodyne beat of two Nd:YAG lasers independently locked to two 20-cm cavities. (a) Beat frequency; (b) frequency instability. A linear drift of 0.016 Hz/s is removed from the beat frequency.

To measure the frequency noise of the system, each Nd:YAG laser is locked to its own 20-cm optical cavity. The heterodyne beat between two locked lasers is downconverted and then measured by a frequency counter. The noise spectrum of the beat is given in Fig. 3(b). At 1 mHz, the frequency noise is 3.5 $\mathrm{Hz}/\sqrt{\mathrm{Hz}}$, and in the measured frequency range of 100 μHz–0.5 Hz, it is below 20 $\mathrm{Hz}/\sqrt{\mathrm{Hz}}$, which is higher than the thermal noise by factors of 2 to 5.

5. Frequency Stability

Figure 4(a) shows a 12-h time series of the beat note with a linear drift of 0.016 Hz/s removed. The Allan deviations computed from this time series at average time from 0.8 to 6000 s are shown in Fig. 4(b). The frequency instability of the heterodyne beat is reduced to 3.0×10^{-16} (2.1×10^{-16}, a single laser) around 1 s, and it remains below 5.0×10^{-16} (3.5×10^{-16}, a single laser) at an average time of up to 6000 s.

Finally, we note that the frequency drift of the cavity should be further investigated for space applications, especially for those in which long-term frequency stability is crucial. Although the relative drift rate of our two 20-cm ultrastable cavities gradually settled down since their first operation, in a zero-g environment, the drift rate can be different from its ground value even if enough relaxation time is allowed. One possible laboratory test is to check for a potential change in the steady-state drift rate after the cavity orientation is deliberately altered from horizontal to vertical.

6. Conclusion

As an important step toward an ultrastable laser for space-based GW detection, an FPGA-based laser frequency-locked system is developed and tested. To evaluate its performance, the system

is employed to lock a spaceborne 1064 nm NPRO Nd:YAG laser to a laboratory-operated 20-cm ultrastable cavity. The optical power of the laser in front of the cavity is actively stabilized, and the RIN measured in front of the cavity is reduced to $8.0\times10^{-3}/\sqrt{\text{Hz}}$ (100 μHz) − $4.0\times10^{-4}/\sqrt{\text{Hz}}$ (0.5 Hz). Feedback control of RAM originating in the waveguide EOM is also adopted, reducing its contribution to levels below thermal noise limit. The heterodyne beat between two independently operated systems shows that the frequency noise is 3.5 $\text{Hz}/\sqrt{\text{Hz}}$ at 1 mHz, and the corresponding frequency stability is 3.0×10^{-16} (2.1×10^{-16}, a single laser) around 1 s and stays at the level of 10^{-16} for 6000 s, demonstrating the potential of the FPGA-based locked system to achieve a 10^{-16} level of frequency stability. Currently, we are developing a space-version reference cavity that adopts ULE mirrors (one flat and one concave with an ROC of 0.5 m) and has a reduced length of 7.5 cm due to constraints on volume and weight. This cavity shows a higher level of thermal noise (~10 $\text{Hz}/\sqrt{\text{Hz}}$ at 1 mHz) compared with the 20-cm cavity[29]. To suppress low-frequency noises, precision temperature stabilization and thermal shields will be adopted. This reference cavity, together with the developed NPRO Nd:YAG laser and FPGA-based control unit, will realize an ultrastable laser whose frequency noise is below 30 $\text{Hz}/\sqrt{\text{Hz}}$ (1 mHz–1 Hz), satisfying the requirement of the space GW detection.

Acknowledgements

This work was supported by the National Key Research and Development Program of China (Nos. 2021YFC2201800 and 2020YFC2200300), the National Natural Science Foundation of China (Nos. 11327407, 11654004, and 11235004), and the Strategic Priority Research Program of the Chinese Academy of Sciences (Nos. XDB21010300 and XDB23030202).

References

1. B. C. Young, F. C. Cruz, W. M. Itano, *et al.*, "Visible lasers with subhertz linewidths," Phys. Rev. Lett. **82**, 3799 (1999).
2. B. P. Abbott, R. Abbott, T. D. Abbott, *et al.*, "Observation of gravitational waves from a binary black hole merger," Phys. Rev. Lett. **116**, 061102 (2016).
3. K. Danzmann and the LISA Study Team, "LISA— an ESA cornerstone mission for the detection and observation of gravitational waves," Adv. Space Res. **32**, 1233 (2003).
4. S. Häfner, S. Falke, C. Grebing, *et al.*, "8×10^{-17} fractional laser frequency instability with a long room-temperature cavity," Opt. Lett. **40**, 2112 (2015).
5. W. Zhang, J. M. Robinson, L. Sonderhouse, *et al.*, "Ultrastable silicon cavity in a continuously operating closed-cycle cryostat at 4 K," Phys. Rev. Lett. **119**, 243601 (2017).
6. Q. Chen, E. Magoulakis, and S. Schiller, "High-sensitivity crossed-resonator laser apparatus for improved tests of Lorentz invariance and of space-time fluctuations," Phys. Rev. D **93**, 022003 (2016).
7. R. Xiao, Y. Xu, Y. Wang, *et al.*, "Transportable 30 cm optical cavity based ultrastable lasers with beating instability of 2×10^{-16}," Appl. Phys. B **128**, 220 (2022).
8. C. Yan, H. Shi, Y. Yao, *et al.*, "Automatic, long-term frequency-stabilized lasers with sub-hertz linewidth and 10^{-16} frequency instability," Chin. Opt. Lett. **20**, 070201 (2022).
9. J. Bu, D. Jiao, G. Xu, *et al.*, "Fast auto-relock methods for ultra-stable lasers," Infrared Phys. Technol. **134**, 104915 (2023).
10. Y. Luo, H. Li, and H.-C. Yeh, "Note: Digital laser frequency auto-locking for inter-satellite laser ranging," Rev. Sci. Instrum. **87**, 056105 (2016).
11. A. Roy, L. Sharma, I. Chakraborty, *et al.*, "An FPGA based all-in-one function generator, lock-in amplifier and auto-relockable PID system," J. Instrum. **14**, P05012 (2019).
12. A. Didier, S. Ignatovich, E. Benkler, *et al.*, "946-nm Nd:YAG digital-locked laser at 1.1×10^{-16} in 1 s and transfer-locked to a cryogenic silicon cavity," Opt. Lett. **44**, 1781 (2019).
13. W. Zhang, M. J. Martin, C. Benko, *et al.*, "Reduction of residual amplitude modulation to 1×10^{-6} for frequency modulation and laser stabilization," Opt. Lett. **39**, 1980 (2014).
14. G. Mueller, P. McNamara, I. Thorpe, *et al.*, "Laser frequency stabilization for LISA," https://ntrs.nasa.gov/api/citations/20060012084/downloads/20060012084.pdf (2005).
15. G. Heinzel, C. Braxmaier, K. Danzmann, *et al.*, "LISA interferometry: recent developments," Class. Quantum Grav. **23**, S119 (2006).
16. J. Stacey, G. P. Barwood, A. Spampinato, *et al.*, "Laser frequency stabilisation for the LISA mission using a cubic cavity," Proc. SPIE **12777**, 266 (2023).
17. B. Bachman, G. De Vine, J. Dickson, *et al.*, "Flight phasemeter on the Laser Ranging Interferometer on the GRACE Follow-On mission," J. Phys. Conf. Ser. **840**, 012011 (2017).
18. M. Tinto and J. W. Armstrong, "Cancellation of laser noise in an unequal-arm interferometer detector of gravitational radiation," Phys. Rev. D **59**, 102003 (1999).
19. D. A. Shaddock, B. Ware, R. E. Spero, *et al.*, "Postprocessed time-delay interferometry for LISA," Phys. Rev. D **70**, 081101(R) (2004).
20. G. de Vine, B. Ware, K. McKenzie, *et al.*, "Experimental demonstration of time-delay interferometry for the laser interferometer space antenna," Phys. Rev. Lett. **104**, 211103 (2010).
21. M. Tinto and S. V. Dhurandhar, "Time-delay interferometry," Living Rev. Relativ. **24**, 1 (2020).
22. G. Wang and W. Ni, "Time-delay interferometry for ASTROD-GW," Chin. Astronom. Astrophys. **36**, 211 (2012).
23. J. Peng, L. Li, and L. Chen, and On behalf of The Taiji Scientific Collaboration, "A spaceborne neodymium-doped yttrium aluminum garnet laser with nonplanar-ring-oscillator configuration," Int. J. Modern Phys. A **36**, 2140007 (2021).
24. L. Li, J. Wang, J. Bi, *et al.*, "Ultra-stable 1064-nm neodymium-doped yttrium aluminum garnet lasers with 2.5×10^{-16} frequency instability," Rev. Sci. Instrum. **92**, 043001 (2021).
25. R. W. P. Drever, J. L. Hall, F. V. Kowalski, *et al.*, "Laser phase and frequency stabilization using an optical resonator," Appl. Phys. B **31**, 97 (1983).
26. F. Allard, I. Maksimovic, M. Abgrall, *et al.*, "Automatic system to control the operation of an extended cavity diode laser," Rev. Sci. Instrum. **75**, 54 (2004).
27. E. L. Wooten, K. M. Kissa, A. Yi-Yan, *et al.*, "A review of lithium niobate modulators for fiber-optic communications systems," IEEE J. Sel. Top. Quantum Electron. **6**, 69 (2000).
28. N. C. Wong and J. L. Hall, "Servo control of amplitude modulation in frequency-modulation spectroscopy: demonstration of shot-noise-limited detection," J. Opt. Soc. Am. B **2**, 1527 (1985).
29. K. Numata, A. Kemery, and J. Camp, "Thermal-noise limit in the frequency stabilization of lasers with rigid cavities," Phys. Rev. Lett. **93**, 250602 (2004).